Determination of mobilized asperity parameters to define rock joint shear strength in low normal stress conditions

D.H. Kim[1], I. Gratchev[2], A.S. Balasubramaniam[3] and M. Chung[4]

[1]Faculty of Griffith School of Engineering, Griffith University, G09_1.46, 4222, Gold Coast, QLD, Australia; PH (61) 7555-27810; FAX (61) 7555-28065; email: donghyun.kim@griffith.edu.au
[2]Faculty of Griffith School of Engineering, Griffith University, G09_1.15, 4222, Gold Coast, QLD, Australia; PH (61) 7555-27686; FAX (61) 7555-28065; email: i.gratchev@griffith.edu.au
[3]Faculty of Griffith School of Engineering, Griffith University, G09_1.46, 4222, Gold Coast, QLD, Australia; PH (61) 7555-27810; FAX (61) 7555-28065; email: a.bala@griffith.edu.au
[4]Faculty of Griffith School of Engineering, Griffith University, G09_1.46, 4222, Gold Coast, QLD, Australia; PH (61) 7555-27810; FAX (61) 7555-28065; email: matthew.chung@griffithuni.edu.au

ABSTRACT

This paper describes the role of mobilized asperity angles in shear behaviour of weak rock joints based on the results of direct shear tests using roughness profiles in 1mm intervals. Matched joint sets of plaster casts, which simulate Barton's typical joint roughness profiles, are created for the tests. In order to simulate accurate asperities with the same intervals, special moulds are produced by a 3D printing technique. Based on the measured compressive strength of the plaster casts, the direct shear tests are performed under low normal stress conditions.

The interpretation of the test data demonstrates a parameter which is the relationship between the mean values of mobilized asperity angles in damaged areas to the asperity component of Barton's shear strength criterion. In low normal stress conditions, Baton's criterion, combined with the proposed parameter, shows high correlation with the test results. This indicates that the shear behaviour of joints is governed by the partly mobilized asperities in low normal stress conditions. As a result, the parameter has a linear relationship with the joint roughness coefficients according to the normal stresses and the compressive strength of the plaster materials. As the parameter is obtained from the asperity angles estimated by 1mm intervals, this can correlate with measured roughness profiles obtained by manual or remote sensing methods.

Keywords: JRC, average asperity angles, mobilized asperity parameter, 3D printing

1   INTRODUCTION

The shear behaviour of rock joints is largely dependent on the degree of roughness of the shearing surfaces. In two dimensional conditions, the roughness profiles can be described as both large scale waviness and small scale unevenness. In low normal stress conditions, the shear behaviour of rock joints is initiated rather by degradation of small scale roughness components (unevenness) than by large scale waviness (Patton, 1966). In this case, the shear strength of joints is governed by the mobilized asperities which are induced by the contact areas during shear stages (Barbosa, 2009). In order to identify the role of the employed roughness in shearing stages, Barton (1982) introduced the concept of a mobilized joint roughness coefficient (JRC_{mob}) which defines the contribution of roughness over the whole shearing process.

The mobilized asperity angles and the damaged areas are generally revealed after shearing, and these components have a direct influence on the mobilized JRC values. Thus, this study investigates the role of mobilized average asperity angles in damaged areas during shearing stages by conducting a considerable number of experiments. The asperity angles of rock joints vary with the size of the intervals (Rengers,1970; Bandis,1980). However, JRC values are traditionally estimated by comparing the measured in the joint profiles. These are measured by a profile gauge (1mm comb interval), with typical roughness profiles for both laboratories and field surveys. Due to the fact that roughness profiles in the same scale (1mm interval) can be obtained from manual measurements or remote sensing methods such as photogrammetry (Haneberg, 2007; Poropat, 2009; Kim et al., 2013), a one millimetre interval between steps can be assumed to be the optimum size for examining the influence of asperity angles on rock joint shear behaviour.

In experimental studies, plaster, which can be moulded into any shape of asperities when mixed with water, have been used for simulations of rock joint roughness by many researchers (Kodikara et al., 1994; Indraratna, 1998; Homand et al., 2001; Yang et al., 2001; Jafari et al., 2003; Budi et al., 2014). However, most studies have focused more on the shear behaviour of saw-tooth asperity shapes. This can be explained by there having been difficulties in creating custom made small scale roughness components in the plaster casts for this study. Thus, the results of these experiments will be as accurate as possible.

In this study, direct shear tests are performed using matching plaster sets. In order to simulate accurate asperities of the typical JRC profiles, special plate casts, which simulate 1mm interval roughness coordinates, are created by a 3D printing method. The sets of casts are able to produce well matched joint sets of plasters. In addition, two different strength plaster casts, which are Hydrocal (high strength) and dental cement (low strength), are used to investigate the differences of mobilized asperities according to their strengths. The strength properties of the plaster casts are also determined by point load strength tests and unconfined compressive strength tests. This study suggests a parameter which is the ratio of the average mobilized asperity angles in damaged areas to the asperity component of Barton's equation. The parameter can be applied to Barton's shear strength criterion for weak rock joints in low normal stress conditions.

2   MOBILIZED ASPERITY ANGLES IN DAMAGED AREAS

The bilinear model regarding regular saw tooth inclination, which accounts for the function of asperity angles in rock joint shear strength, was previously proposed by Patton (1966) as given below:

$$\tau = \sigma_n \tan(\phi_r + i) \tag{1}$$

Where, ϕ_r is the residual friction angle and i is the asperity angle of the saw tooth model. It is known that Eq.(1) is valid at low normal stress conditions where shear displacement occurs along the inclined joint surfaces. Using the concept of mobilized joint roughness coefficients (JRC_{mob}) in the mobilized shear strength, Barton (1982) defined the midway shear strength between peak and residual values as presented in Eq. (2). In this concept, the asperity component (i_{est}), which represents the ratio of JRC_{mob} to JRC_{peak}, is estimated by Eq. (3) (Barton, 1982).

$$\tau_{mob} = \sigma_n \tan[(JRC_{mob} log_{10}(JCS/\sigma_n) + \phi_r] \tag{2}$$

$$i_{est} = \phi_p° - \phi_r° = JRC \, log_{10} \, (JCS/\sigma_n) \tag{3}$$

Where, ϕ_p ,ϕ_r are peak and residual friction angles, JCS is joint wall compressive strength, and σ_n is effective normal stress acting on the joint surface. However, in low normal stress conditions, joint shear behaviour tends to be governed by the regions in which asperities come in contact with each other. When shearing is initiated, the contacted areas of the matched joint sets are reduced to the mobilized asperity regions. Then, it can be observed from Figure 1 that the locations of damaged areas during shearing are determined by the sizes of asperity angles for the shear directions. The asperities are damaged during shearing and the shearing mechanism accordingly results in progressively reduced effective asperity angles. Thus, the mobilized asperity angles during shearing directly affect the shear strengths under low normal stresses. In this study, to represent the values of asperities in the mobilized regions, the average asperity angles, i_{ave} in the damaged area, a_d, are employed as shown in Eq.(4).

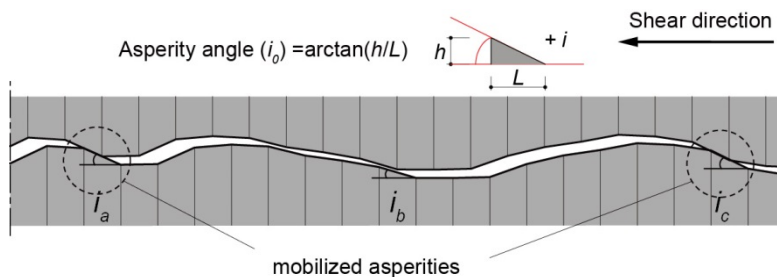$$i_{ave} = \frac{1}{m}\sum_{i=i}^{m} i_d \tag{4}$$

Figure 1. Schematic description of mobilized asperities in shearing

Where, m is the damaged step numbers (1mm step size) during shearing stages and i_d is the asperity angle in every damaged step. The influence of mobilized asperities can be considered by using the average asperity angles and the mobilized asperity factor, λ which is the ratio between average values of mobilized asperity angles and the peak asperity value of Barton's equation as presented in Eq (5). This parameter can be defined as the proportion of the partly mobilized asperities to the fully mobilized asperities in Barton's shear strength criterion under low normal stress condition.

$$\lambda = i_{ave}/i_{est} \tag{5}$$

3 SAMPLE PREPARATION OF RECONSTRUCTED JOINT SETS

3.1 Simulation of joint profiles

In order to create artificial rock joint sets, two types of plaster casts: Hydrocal (high strength) and dental plaster (low strength), are used in this study. The main component of Hydrocal is calcium sulphate hemihydrate ($CaSO_4 \cdot 1/2H_2O$) and Portland cement. The joint surfaces of plaster blocks were created by the replicas obtained from a 3D printing method. To simulate accurate roughness profile shapes, the coordinates of three ranges of Barton's typical joint roughness profiles were digitized in 1 mm intervals and used as input data for the 3D printing system, Project HD3500. The obtained replicas and Project HD3500 system are shown in Figure 2. The corresponding parts of the sets were made by placing silicone on the printed replicas. Then, plaster shear blocks were cured in an acrylic mould.
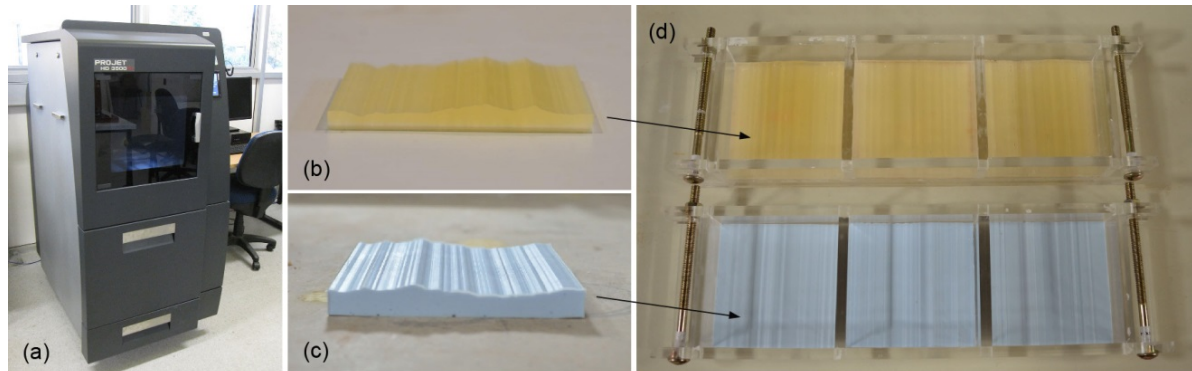

Figure 2. Procedure for replica sample preparation, Project HD3500 (a), Replica obtained from 3D printing (b), Silicone mould (c), Acrylic mould (d)

Three sets of plaster blocks each 100 mm × 100mm × 30mm were created for a range of JRC to carry out direct shear tests under three different normal stresses. The mixing ratios and curing conditions of specimens are described in the next section. The asperity steps on the cured joint surfaces were well simulated in 1mm intervals as shown in Figure 3. The sample sets were created for three different ranges of typical JRC profiles (JRC=4~6, 8~10, 12~14).
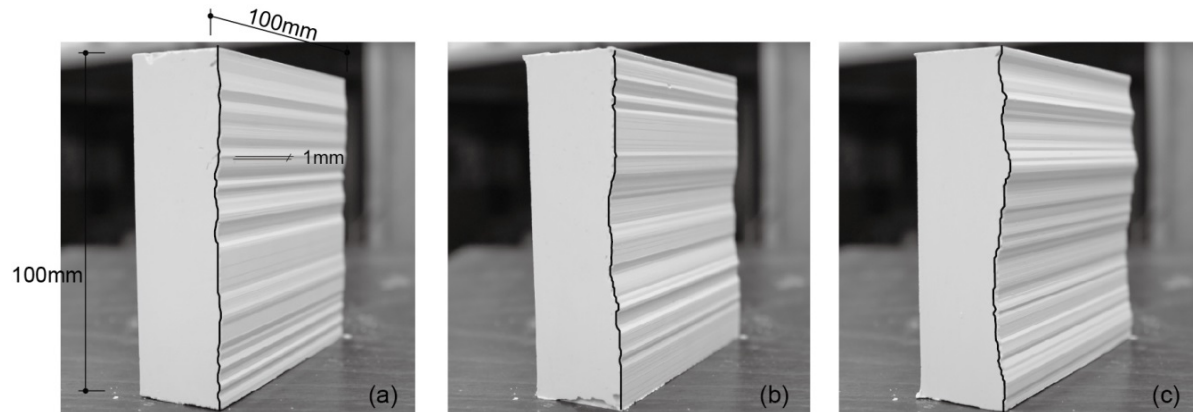

Figure 3. Plaster joint samples, JRC=4~6 (a), JRC=8~10 (b), JRC=12~14

3.2   Strength properties of plasters

To identify the strength properties of the plaster casts, unconfined compressive strength (UCS) tests and point load strength tests (PLT) were performed. The purpose of these tests was to clarify the unconfined compressive strength (UCS) and the tensile strength of the casts using the same curing conditions as with the jointed plaster sets for the shear tests. The plaster samples were made with water-to-cement ratios of 45% for Hydrocal and 60% for dental cement respectively. The UCS tests and the PLT tests used 100mm cubic shapes for UCS and 50mm cubic shapes for PLT.

To obtain the most effective curing condition for the casts, a total of 24 UCS tests and 24 PLT tests were performed for Hydrocal and dental cement. The samples were cured in an oven at four different curing temperatures: 30°C, 50°C, 75°C and 100°C and the degree of drying was determined by measuring the weight of the samples stored in the oven each day. The test results show that the PLT and UCS strength values of both types of casts continue to drop as curing temperature increase; thereby resulting in brittle failure. The reduction in strength is noticeable at less than 75°C of curing temperature (see Figure 4 (b)). This agrees with an idea that the curing temperature should be less than 50°C, because high temperatures can initiate shrinkage cracking in the samples (Indraratna, 1990). The correlative relationships between the point load strength index and the unconfined compressive strength are also shown in Figure 4 (c).

According to the results of high temperature outcomes for PLT and UCS, the artificial joint sets for shear tests are cured at 30°C in the oven for 1 week to obtain higher strengths. The curing time was determined by considering the drying time for both types of casts (see Figure 4 (a)). The results of the strength tests and the material properties are presented in Table 1.
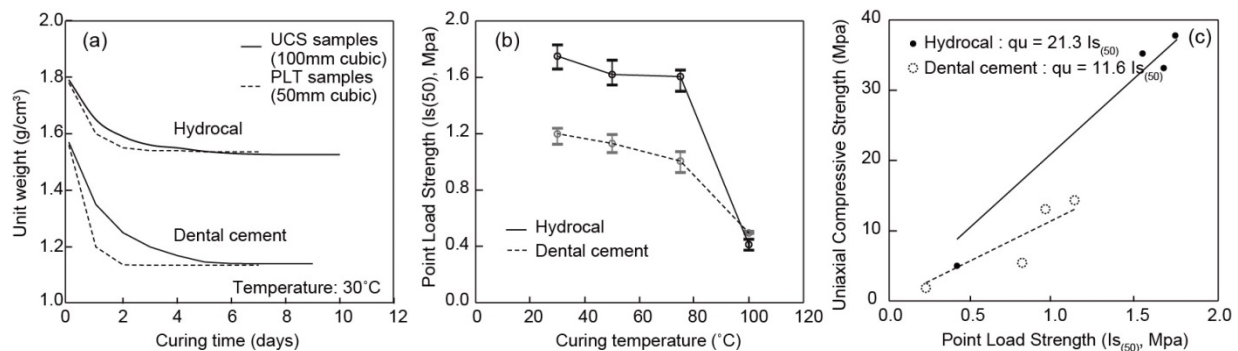

Figure 4. Results of tests, drying curves (a), PLT tests (b) and UCS tests (c)

Table 1:   Properties of plaster samples for UCS and PLT tests (at 30°C)

Plaster materials	High strength plaster (Hydrocal)	Low strength plaster (dental cement)
Specific Gravity	2.96	2.63
Unit weight (g/cm³)	1.51 ~ 1.54	1.11 ~ 1.15
Unconfined compressive strength (Mpa)	36.8 ~ 39.1	14.1 ~ 14.6
Point load strength (Is(50), Mpa)	1.65 ~ 1.82	1.12 ~ 1.23

4   SHEAR BEHAVIOUR OF TYPICAL ROUGHNESS PROFILES

4.1   Direct shear tests

Direct shear tests were performed using a portable shear apparatus (see Figure 5). Nine sets of Hydrocal replicas and nine sets of dental cement replicas were sheared in three normal stress levels ranging from 0.1MPa to 0.3MPa. The total shear displacement is about 10 mm which is 10% of the specimen length. The shear tests are limited by the low normal stress conditions due to the characteristics of casts which are largely responsible for their low strengths and brittle behaviours. Thus, when a shear stress is applied on the rough surface joints, sliding can occur by climbing along the stress bearing faces of the asperities. Sample rotation during shearing stages can affect the shear behaviour. However, its rotation was ignored because it was observed that rotation is prevented by the stable sample setting due to the shapes of plaster casts.
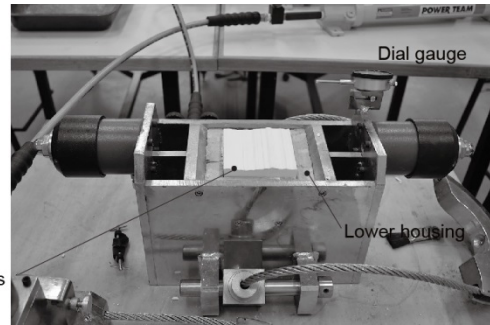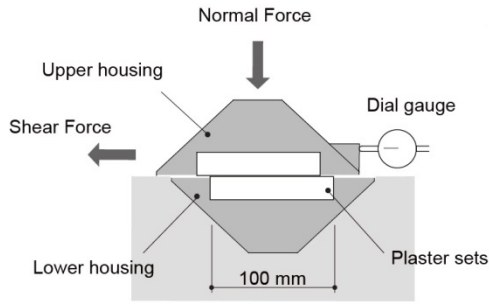
Figure 5. Direct shear apparatus and plaster samples setting

During the process of shearing, brittle failure, which was induced by concentrated tensile stresses, occurred in the samples especially when higher normal stresses were applied. Accordingly, the major asperities, which have the steepest angles in the roughness profiles, are completely sheared at the highest normal stress levels in the entire range of joint sets. The nature of the failure can be observed from the failure surfaces. Breakages of brittle surfaces caused by shear tension in the plaster samples are shown in Figure 6. It was observed that this brittle failure tends to be shown more in Hydrocal samples than in dental cement samples. Further, the strength curves of both casts distinguish the differences of their strengths. In the case of Hydrocal, the linearity of the stress-displacement curves increased rapidly and dropped sharply in the shear strength curves due to the shearing some of the asperities. On the other hand, the shear stress curves for the dental casts indicate a smoother inclination to the peak shear stress values compared to the behaviour of Hydrocal as shown in Figure 6.

After shearing the damaged regions are identified from observations on the sheared surfaces of the samples. As a result, the areas showed a damage range from grinding to breaking and the size of the areas could be evaluated by tracing the perimeters of the sheared parts of the joint surfaces. When shearing was initiated, the joint surfaces became mismatched and the contact area was reduced. At the same time, the major asperities started to fail, showing some debris of sheared asperities. It was found that the peak shear stress was observed from the damage on the major asperities. However, most other asperities were undamaged or showed only minor damage.

Figure 7 shows the major asperities of the three selected joint sets for the shear direction. The direct shear tests distinctly demonstrate the distributions of damaged areas centred by the major asperities of the joint profiles. Figure 8 demonstrates the growth of the damaged areas as normal stress increased.
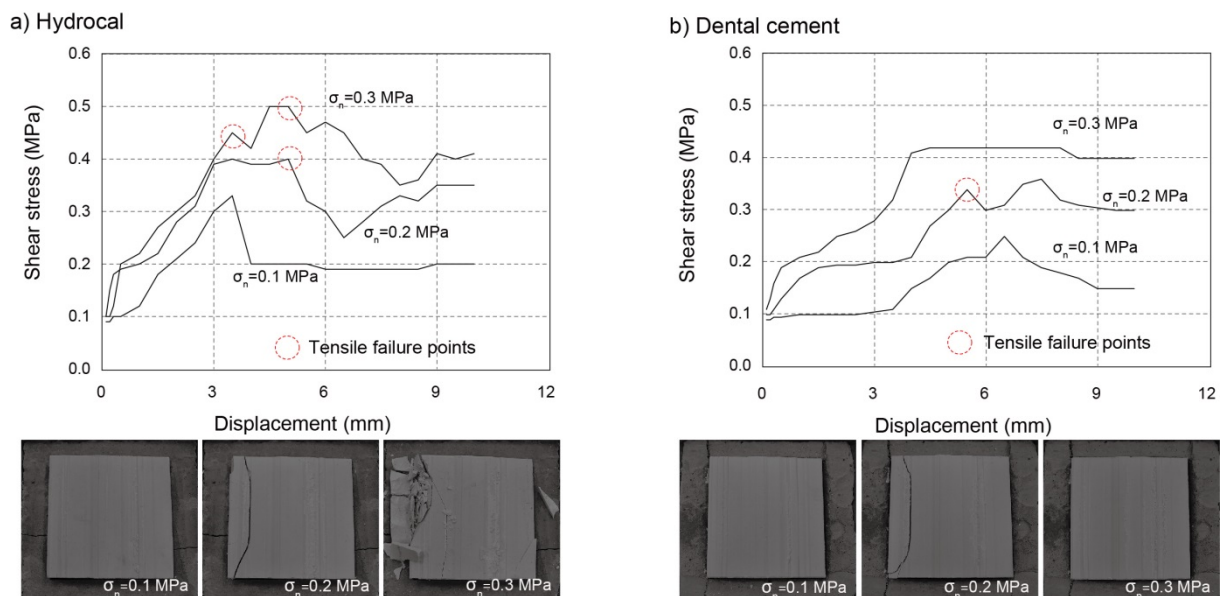

Figure 6. Influence of tensile failures during shearing (JRC: 8~10), Hydrocal (a), dental cement (b)
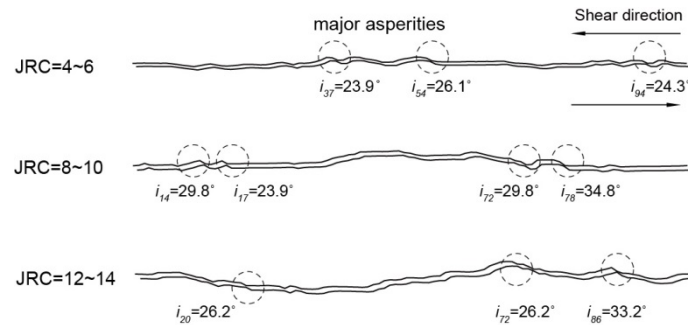
Figure 7. Major asperities in the ranges of JRC profiles

The results indicate a clear trend that the measured damaged areas (a_d) increased with the normal stresses, even though the two halves of the jointed plaster casts were not perfectly mated. To estimate the sizes and step numbers of the damaged areas accurately by observation, digital photographs, which were taken before and after the shearing stages, were used to trace the damaged areas. The images were converted into greyscale images and the brightness and contrast of the images were adjusted to highlight distinct borders of damaged areas. It was found that the extent of the damaged area depends on the extent of the asperity angles in the direction of the shear.

The average mobilized asperity angles, i_{ave}, in the damaged areas are presented in Table 2. The numbers of damaged steps in 1mm intervals in the damaged areas were used for calculating the average asperity angles. These values are mostly reduced ranging from 16° to 24° as normal stresses increased and as the damaged areas enlarged. The results show that the number of damaged steps increases with normal stress and the dental plaster step numbers are larger than those of Hydrocal in all JRC ranges. However, there is no trend within JRC values. These values represent the mobilized asperities which play a direct role in revealing the peak shear strength for the mobilized regions.
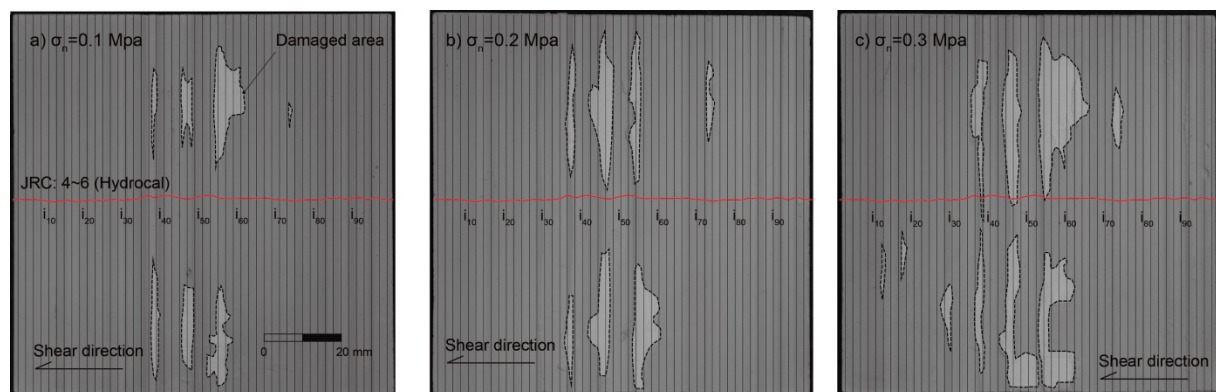

Figure 8. Damaged areas after shearing with different normal stresses (Hydrocal, JRC:4~6)

Table 2:   Damaged steps and average asperity angles in the damaged areas

Plasters			Hydrocal			dental cement		
JRC ranges			4~6	8~10	12~14	4~6	8~10	12~14
Normal stress (Mpa)	0.1	**Damaged steps**	4	8	3	6	8	4
		i_{ave}	20.0˚	23.7˚	17.9˚	17.1˚	23.7˚	24.4˚
	0.2	**Damaged steps**	5	9	7	8	9	7
		i_{ave}	18.3˚	22.3˚	23.0˚	16.2˚	22.3˚	21.4˚
	0.3	**Damaged steps**	6	12	6	8	7	10
		i_{ave}	17.5˚	20.4˚	21.2˚	16.2˚	22.4˚	22.1˚

4.2   Discussion on the test results

Using the average values of asperity angles, the mobilized asperity factors, λ, are estimated and plotted according to the JRC values in Figure 9. In the tested JRC ranges, this parameter, λ shows a linear relationship with JRC values based on their compressive strengths. The values varied from around 1.7 to 0.8 in the Hydrocal samples, while the JRC values increase from 5 to 14. If the value of

λ is more than 1, the average asperity angle is higher than Barton's asperity component value. This means that the shear strength of joints can be affected by partly the mobilized asperities in Barton's equation. Thus, this parameter can be a contributor in Barton's original equation as follows.

$$\tau_{mob} = \sigma_n \tan[(JRC_{peak} \cdot \lambda \cdot log_{10}(JCS/\sigma_n) + \phi_r] \tag{6}$$

The parameter, λ, is defined as a function of JRC values and the compressive strength of rocks. It can be seen from the test results that dental plaster, which has a lower compressive strength than Hydrocal, has higher values of λ for the same JRC profiles.
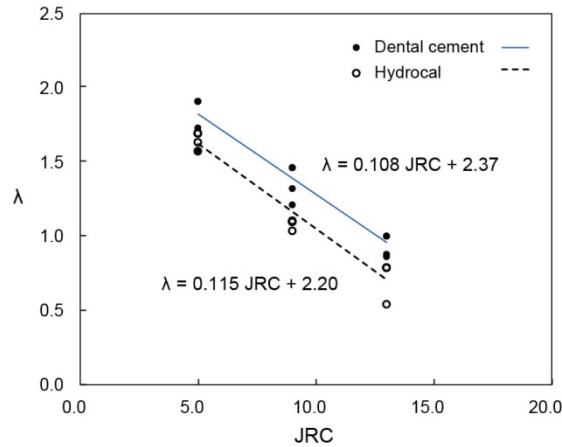

Figure 9. Relationship between influential factor (λ) and JRC

The results of direct shear tests and the shear strength criterion which were defined by Barton (1982) are compared in Figure 10. The result shows that Barton's function tends to underestimate the shear strength in low JRC ranges (JRC=4~6), and to overestimate the values in high JRC ranges (JRC=12~14). On the other hand, the proposed function in Eq.(6) regarding the mobilized asperity parameter , λ, shows relatively good agreement between the predictions and the experimental data in the low normal stress condition compared to the original Barton's equation. The test results represent the behaviour of low strength artificial rock samples. However, the idea of using this parameter for estimating joint shear strength can extend to natural rock conditions. Additional study is needed to further define and modify this parameter for natural rock samples.
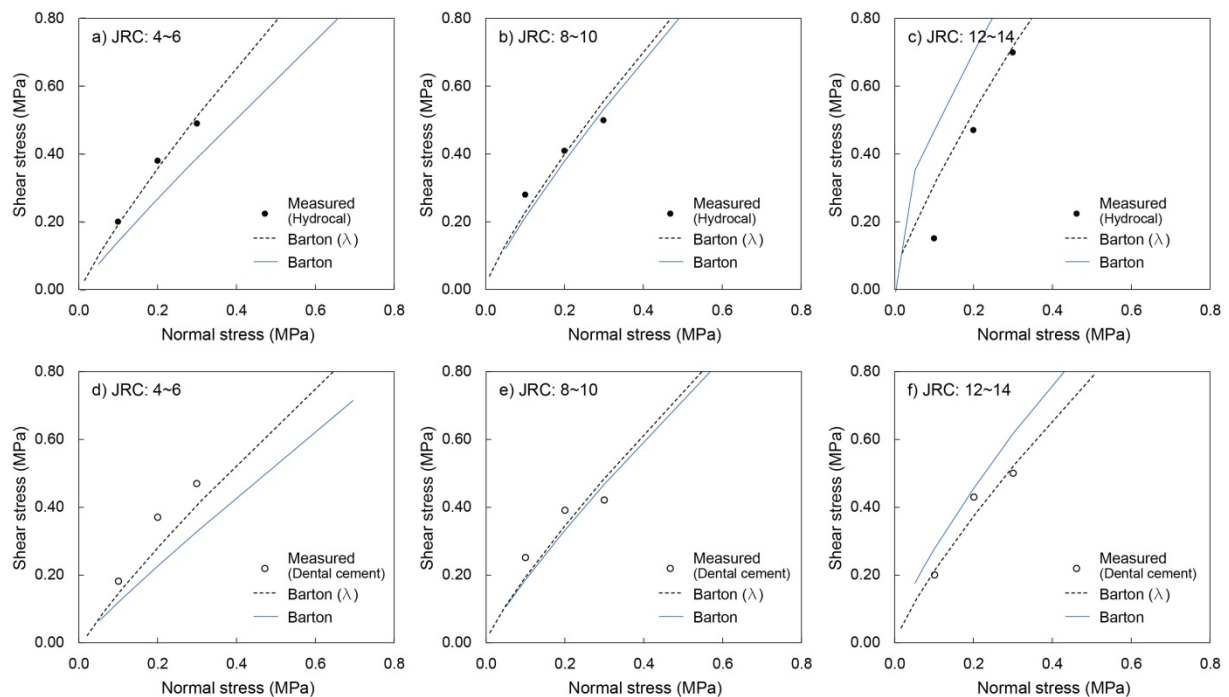

Figure 10. Comparing the rock joint shear criterion

5   CONCLUSION

This study proposes a method to estimate the average asperity angle, i_{ave} in damaged areas and the mobilized asperity factor, λ, which is a ratio of the mean values of mobilized asperities to the asperity component of Barton's criterion. A series of direct shear tests was performed using plaster casts which could represent weak rocks. The artificial joint sets for the tests were simulated with Barton's typical roughness profiles in 1mm intervals and the specimens were created by a 3D printing method.

The results of this study show that the asperities with 1mm step sizes are well simulated using the 3D printing method. Higher strength plaster casts were able to be created during a 1 week curing time at below 30˚C of oven temperature. The results of direct shear tests indicate that the mobilized asperity factor, which is estimated by the average values of asperity angles in 1mm step sizes in damaged areas, is a function of JRC values and the compressive strength of the material. Barton's equation combining the mobilized asperity factor, λ shows reasonably good consistency with the measurement data in low normal stress conditions.

REFERENCES

Bandis, S. (1980). "Experimental studies of scale effects on shear strength and deformation of rock joints." PhD thesis, Univ of Leeds.

Barbosa, R. E. (2009). "Constitutive model for small rock joint samples in the lab and large rock joint surfaces in the field." Proc. 3rd CANUS Rock Mechanics Symposium, Toronto, Paper 5000.

Barton, N. (1982). "Modelling rock joint behaviour from in situ block tests: implications form nuclear waste repository design." Office of Nuclear Waste Isolation, Columbus, Ohio, ONWI-260.

Budi, G., Rao, K. U. M., Deb, D. (2014). "Laboratory modelling of rock joints under shear and constant normal loading." International Journal of Research in Engineering and Technology, 3(4), 190-200.

Haneberg, W. C. (2007). "Directional roughness profiles from three-dimensional photogrammetric or laser scanner point clouds. Proc. 1st Canada-U.S. Rock Mechanics symposium, Vancouver, 101-106.

Homand, F., Belem, T., Souley, M. (2001). "Friction and degradation of rock joint surfaces under shear loads." Int J Numer Anal Meth Geomech, 25, 973-999.

Indraratna, B. (1990). "Development and applications of a synthetic material to simulate soft sedimentary rocks." Géotechnique, 40(2), 189-200.

Indraratna, B., Haque, A., Aziz, N. (1998). "Laboratory modelling of shear behaviour of soft joints under constant normal stiffness conditions." Geotechnical and Geological Engineering, 16, 17-44.

Jafary, M. K., Amini Hosseine, K., Pellet, F., Boulon, M., Buzzi, O. (2003). "Evaluation of shear strength of rock joints subjected to cyclic loading." Soil Dynamics and Earthquake Engineering, 23, 619-630.

Kim, D. H., Gratchev, I., Poropat, G. V. (2013). "The determination of joint roughness coefficient using three-dimensional models for slope stability analysis." Proc. Australian Centre for Geomechanics, Slope Stability 2013, Brisbane, 281-289.

Kodikara, J. K., Johnston, I. W. (1994). "Shear behaviour of irregular triangular rock-concrete joints." Int J Rock Mech Min Sci & Geomech Abst, 31(4), 313-322.

Patton, F.D. (1966). "Multiple modes of shear failure in rocks." Proc. 1st Cong, Int. Soc Rock Mech., Lisbon (1), 509-513.

Poropat, G. V. (2009). "Measurement of surface roughness of rock discontinuities." Proc. 3rd CANUS Rock Mechanics Symposium, Toronto

Rengers, N. (1970). "Influence of surface roughness on the friction properties of rock planes." Proc. 2nd Cong Int Soc Rock Mech., Belgrad (I), 229-234.

Yang, Z. Y., and Chiang, D. Y. (2000). "An experimental study on the progressive shear behaviour of rock joints with tooth-shaped asperities." Int J Rock Mech Min Sci, 37, 1247-1259.